

Supporting Information

Preliminary Therapy Evaluation of ^{225}Ac -DOTA-c(RGDyK) Demonstrates that Cerenkov Radiation Derived from ^{225}Ac Daughter Decay Can Be Detected by Optical Imaging for *In Vivo* Tumor Visualization

Darpan N. Pandya¹, Roy Hantgan², Mikalai M. Budzevich³, Nancy D. Kock⁴, David L. Morse⁵, Izadora Batista⁶, Akiva Mintz^{1,6,7}, King C. Li⁷, Thaddeus J. Wadas^{*1,7}

¹Department of Cancer Biology, Wake Forest School of Medicine, Winston-Salem, NC 27157 USA

²Department of Biochemistry, Wake Forest School of Medicine, Winston-Salem, NC 27157 USA

³Small Animal Imaging Laboratory, H. Lee Moffitt Cancer Center & Research Institute, Tampa, FL 33612 USA

⁴Department of Pathology-Section on Comparative Medicine, Wake Forest School of Medicine, Winston-Salem, NC 27157 USA

⁵Department of Cancer Imaging and Metabolism, H. Lee Moffitt Cancer Center & Research Institute, Tampa, FL 33612 USA

⁶Department of Neurosurgery, Wake Forest School of Medicine, Winston-Salem, NC 27157 USA

⁷Department of Radiology, Wake Forest School of Medicine, Winston-Salem, NC 27157 USA

*Corresponding author:

Thaddeus J. Wadas, Ph.D.

Assistant Professor of Cancer Biology and
Radiology

Wake Forest School of Medicine

Medical Center Blvd.

Winston-Salem, NC 27157

phone: (336) 716-5696

fax: (336) 716-0255

e-mail: twadas@wakehealth.edu

Table of Contents

Section	Page Number
Scheme S1. Synthesis of La-DOTA-c(RGDyK)	3
Scheme S2. Radiochemical synthesis of ²²⁵ Ac-DOTA-c(RGDyK)	3
Figure S1. ESI-MS analysis of La-DOTA-c(RGDyK)	4
Figure S2. Reversible two-state bimolecular interaction model for integrin binding	5
Figure S3. Recombinant human $\alpha_v\beta_3$ binding to immobilized c(RGDyK) monitored by surface plasmon resonance spectroscopy	6
Figure S4. La-DOTA-c(RGDyK) inhibition of $\alpha_v\beta_3$:c(RGDyK) binding monitored by surface plasmon resonance spectroscopy	7
Figure S5. Quality control of ²²⁵ Ac-DOTA-c(RGDyK)	8
Table S1. <i>In vitro</i> serum stability of ²²⁵ Ac-DOTA-c(RGDyK)	9
Figure S6. <i>In vitro</i> serum stability of ²²⁵ Ac-DOTA-c(RGDyK) by size exclusion-HPLC	10
Table S2. Biodistribution of ²²⁵ Ac-DOTA-c(RGDyK)	11
Figure S7. Graphical summary: biodistribution of ²²⁵ Ac-DOTA-c(RGDyK)	12
Figure S8. <i>Ex vivo</i> Cerenkov luminescence imaging of selected organs	13
Table S3. Estimated average tumor and kidney dose for animals receiving ²²⁵ Ac-DOTA-c(RGDyK)	14
Figure S9. Maximum tolerated dose and preliminary therapy studies of ²²⁵ Ac-DOTA-c(RGDyK)	15
Figure S10. Histology of select tissues from MTD studies	16

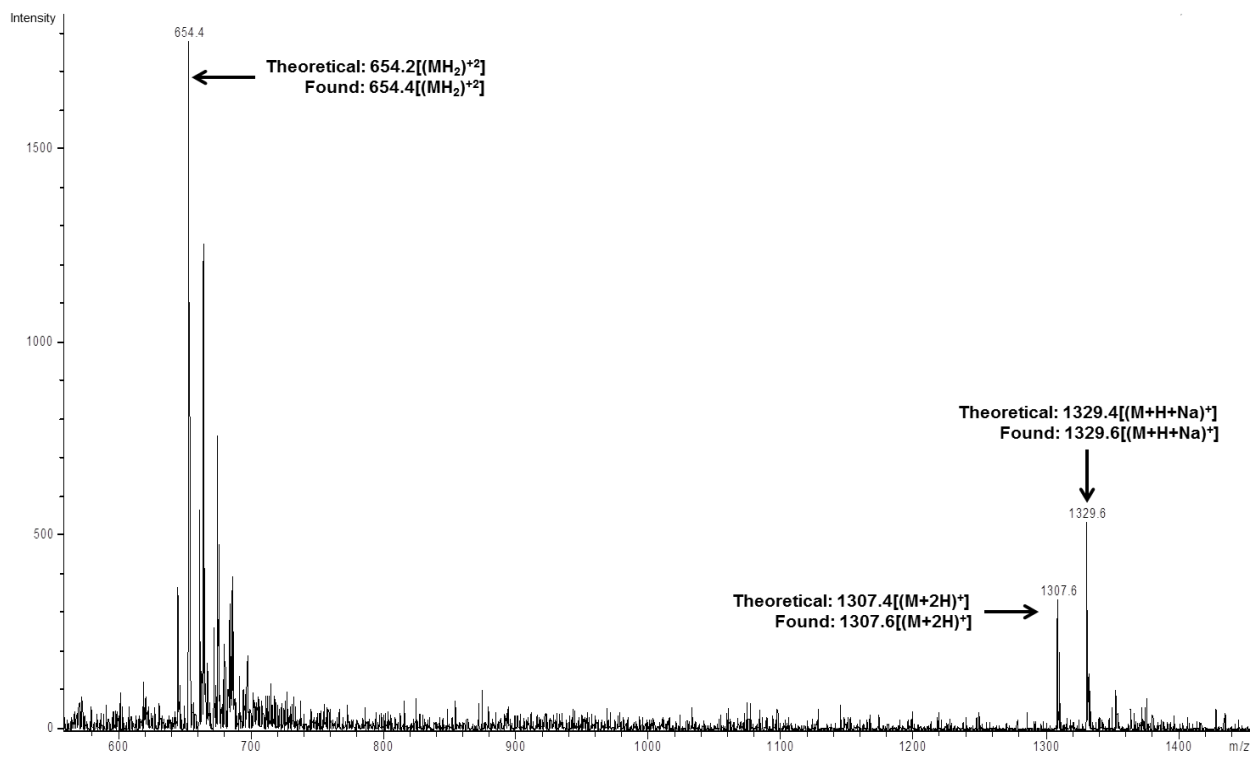


Figure S1. ESI-MS analysis of La-DOTA-c(RGDyK)



Figure S2. Reversible two-state bimolecular interaction model for integrin binding

This model was used to determine the forward (k_{a1} , L/mol-sec) and reverse (k_{d1} , sec^{-1}) rate constants for the initial binding step (indicated by “:”) and forward (k_{a2} , sec^{-1}) and reverse (k_{d2} , sec^{-1}) rate constants for the subsequent stabilizing conformational change (indicated by “*”).

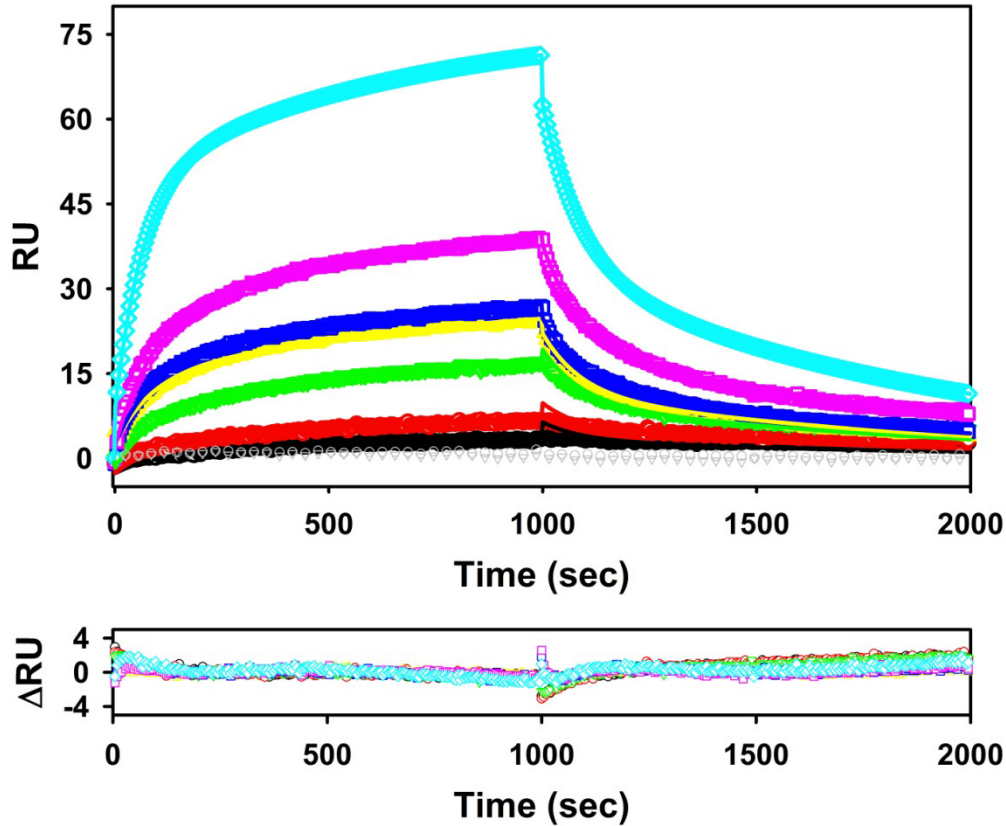


Figure S3. Recombinant human $\alpha_v\beta_3$ binding to immobilized c(RGDyK) monitored by surface plasmon resonance spectroscopy

Increasing concentrations of $\alpha_v\beta_3$ were delivered to c(RGDyK) immobilized on a biosensor chip. Complex formation was measured for 1000 sec; dissociation was monitored for 1000 sec as HBS flowed over the chip. The surface was regenerated with 20 mM EDTA, then 5 M NaCl, prior to the next cycle. Open symbols denote $\alpha_v\beta_3$ concentrations (nM): 3 (black circles), 10 (red circles), 30 (green triangles), 59 (yellow triangles), 83 (blue squares), 100 (red squares), and 300 nM (blue diamonds). Gray symbols denote $\alpha_v\beta_3$ (30 nM) binding data obtained in the presence of excess c(RGDyK) in solution: 11-fold (circles) or 115-fold (triangles). Fitting the complete data set (including 4 $\alpha_v\beta_3$ replicates at 83 nM) to a two-state bimolecular interaction model yielded the solid lines (same color code). Residuals (differences between experimental data and fits) are presented in the same color code in the lower panel.

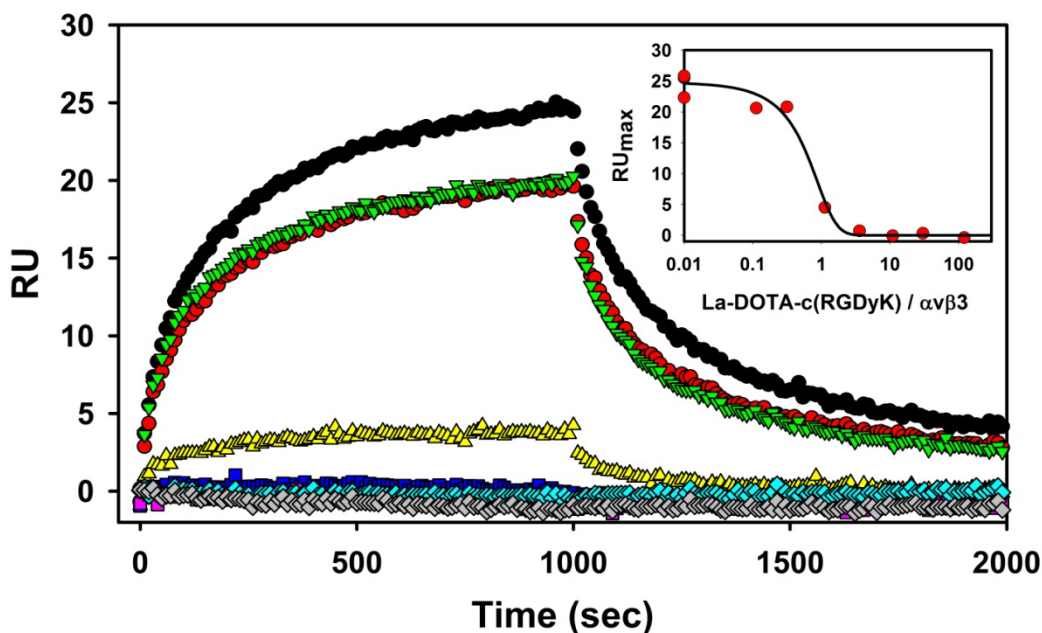


Figure S4. La-DOTA-c(RGDyK) inhibition of $\alpha_v\beta_3$:c(RGDyK) binding monitored by surface plasmon resonance spectroscopy

Samples of $\alpha_v\beta_3$ (83 nM), in the presence of increasing concentrations of La-DOTA-c(RGDyK), were delivered to c(RGDyK) immobilized on a biosensor, while complex formation was measured for 1000 sec. Dissociation was monitored for 1000 sec followed by regeneration. Symbols denote the La-DOTA-c(RGDyK) concentrations (nM): 0 (black), 9.4 (red circles), 26.3 (green triangles), 94 (yellow triangles), 300 (blue squares), 915 (red squares), 2515 (green diamonds), or 10061 (gray diamonds). **Insert:** Maximum RU vs molar excess of La-DOTA-c(RGDyK) over $\alpha_v\beta_3$. Solid line obtained by fitting the complete data set (including 4 $\alpha_v\beta_3$ replicates at 83 nM) to a competitive inhibition model by nonlinear regression, yielding half-maximal inhibition at 0.40 ± 0.16 -fold molar excess.

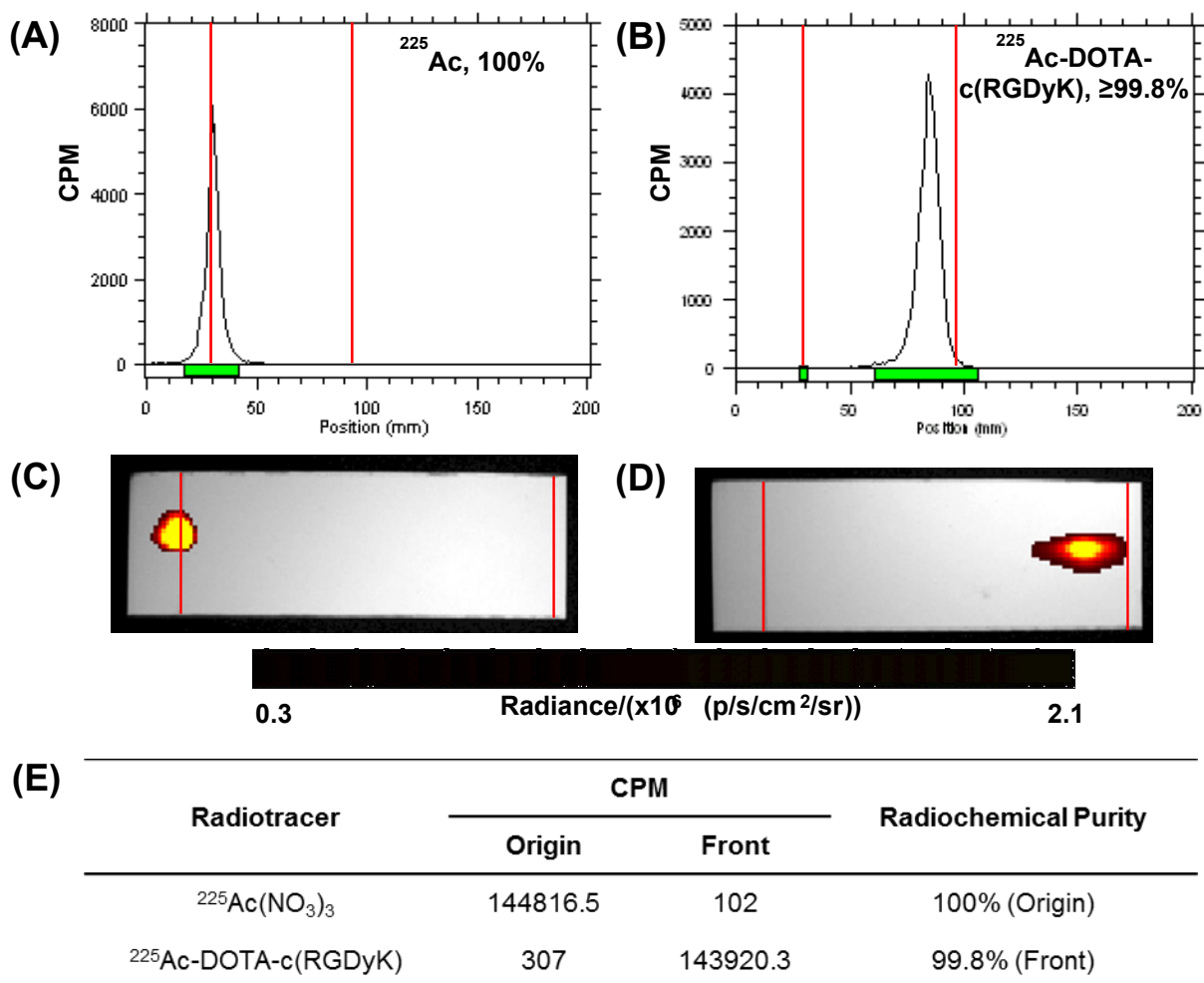


Figure S5. Quality control of $^{225}\text{Ac-DOTA-c(RGDyK)}$

Un-chelated ^{225}Ac remained at the origin ($R_f = 0$) (A); the $^{225}\text{Ac-DOTA-c(RGDyK)}$ moves near the solvent front ($R_f = 0.857$) (B). CLI imaging (C and D) and gamma counting (E) of the TLC plates 24 h after development corroborates the original radio-TLC observations. Based upon all three methods, $^{225}\text{Ac-DOTA-c(RGDyK)}$ has a purity greater than 99.8%.

Table S1. *In vitro* serum stability of ^{225}Ac -DOTA-c(RGDyK) (n = 4)

Day	% Intact of ^{225}Ac-DOTA-c(RGDyK)	
	Radio-TLC scanner	Gamma counter
0	100	100
2	98.9 ± 0.5	98.6 ± 0.4
4	98.1 ± 0.6	97.9 ± 0.7
6	97.4 ± 0.7	97.3 ± 0.5
8	96.6 ± 0.4	96.4 ± 0.6
10	95.7 ± 0.5	95.8 ± 0.3

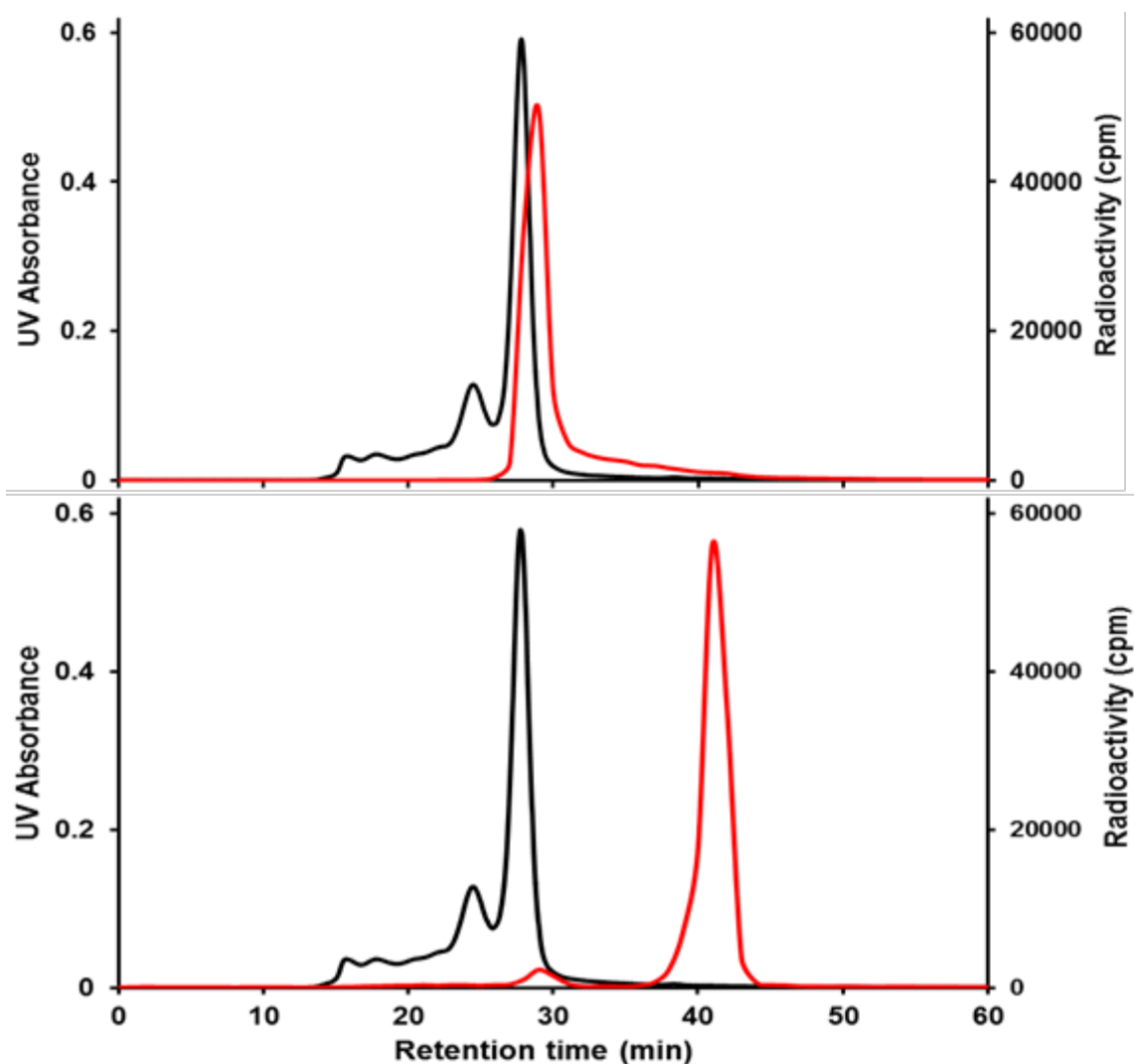


Figure S6. *In vitro* serum stability of $^{225}\text{Ac-DOTA-c(RGDyK)}$ by size exclusion-HPLC

UV-SE-HPLC (220 nm, black) and radio-SE-HPLC chromatogram (red) of $^{225}\text{Ac}(\text{NO}_3)_3$ (top) and $^{225}\text{Ac-DOTA-c(RGDyK)}$ (bottom) in serum after 10 days. Black lines are the UV absorbance due to the human serum components; red lines are the radiotracer associated with ^{225}Ac . Based upon this analysis, only 5% of the activity is transchelated to serum proteins, consistent with the radio-TLC studies.

Table S2. Biodistribution data (mean %ID/g \pm SD) of ^{225}Ac -DOTA-c(RGDyK) at 1 h, 4 h, 4h-blocking, and 24 h post-injection in U87MG tumor-bearing nude mice (n = 6/cohort)

Tissue/Organ	1 h	4 h	4 h-blocking	24 h
Blood	0.318 \pm 0.075	0.028 \pm 0.004	0.013 \pm 0.014	0.006 \pm 0.001
Heart	2.619 \pm 0.483	1.196 \pm 0.352	0.142 \pm 0.070	0.765 \pm 0.365
Lung	6.412 \pm 1.054	1.805 \pm 0.655	0.288 \pm 0.110	0.964 \pm 0.570
Liver	1.885 \pm 0.173	1.746 \pm 0.173	0.430 \pm 0.047	0.902 \pm 0.159
Kidney	5.798 \pm 1.444	2.475 \pm 0.148	1.396 \pm 0.206	1.857 \pm 0.325
Spleen	5.770 \pm 1.361	2.330 \pm 0.648	0.462 \pm 0.191	2.761 \pm 1.309
Pancreas	0.972 \pm 0.157	0.583 \pm 0.231	0.025 \pm 0.030	0.412 \pm 0.039
Stomach	1.373 \pm 0.503	0.879 \pm 0.231	0.074 \pm 0.017	0.433 \pm 0.103
Small Intestine	2.264 \pm 0.152	1.198 \pm 0.194	0.106 \pm 0.022	0.695 \pm 0.088
Large Intestine	1.143 \pm 0.116	1.661 \pm 0.327	0.300 \pm 0.072	0.457 \pm 0.108
Muscle	1.537 \pm 0.367	0.473 \pm 0.282	0.011 \pm 0.012	0.481 \pm 0.150
Fat	0.086 \pm 0.044	0.053 \pm 0.030	0.011 \pm 0.022	0.040 \pm 0.014
Bone	1.749 \pm 0.507	1.346 \pm 0.184	0.585 \pm 0.253	1.014 \pm 0.214
Tumor	3.718 \pm 0.486	2.684 \pm 0.375	0.257 \pm 0.085	1.714 \pm 0.145

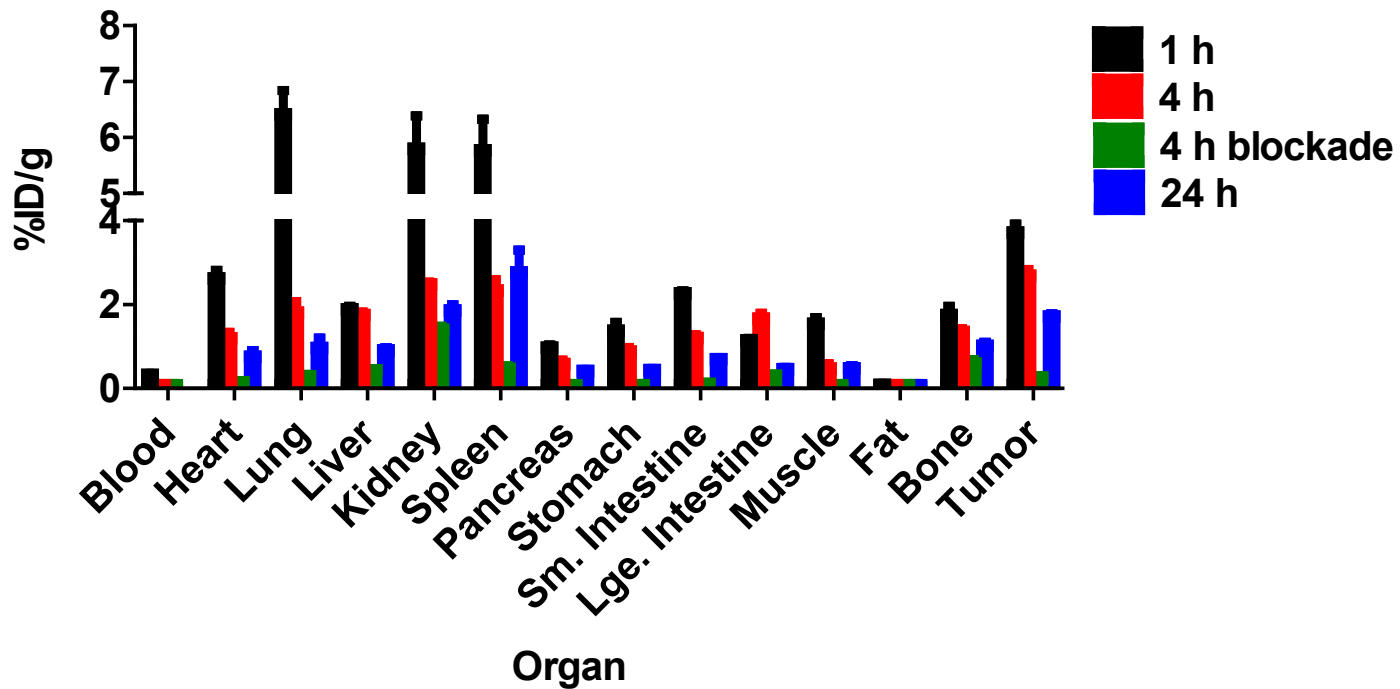


Figure S7. Graphical summary: biodistribution data (mean %ID/g \pm SD) of ^{225}Ac -DOTA-c(RGDyK) at 1 h, 4 h, 4h-blocking, and 24 h post-injection in U87MG tumor-bearing nude mice (n = 6/cohort)

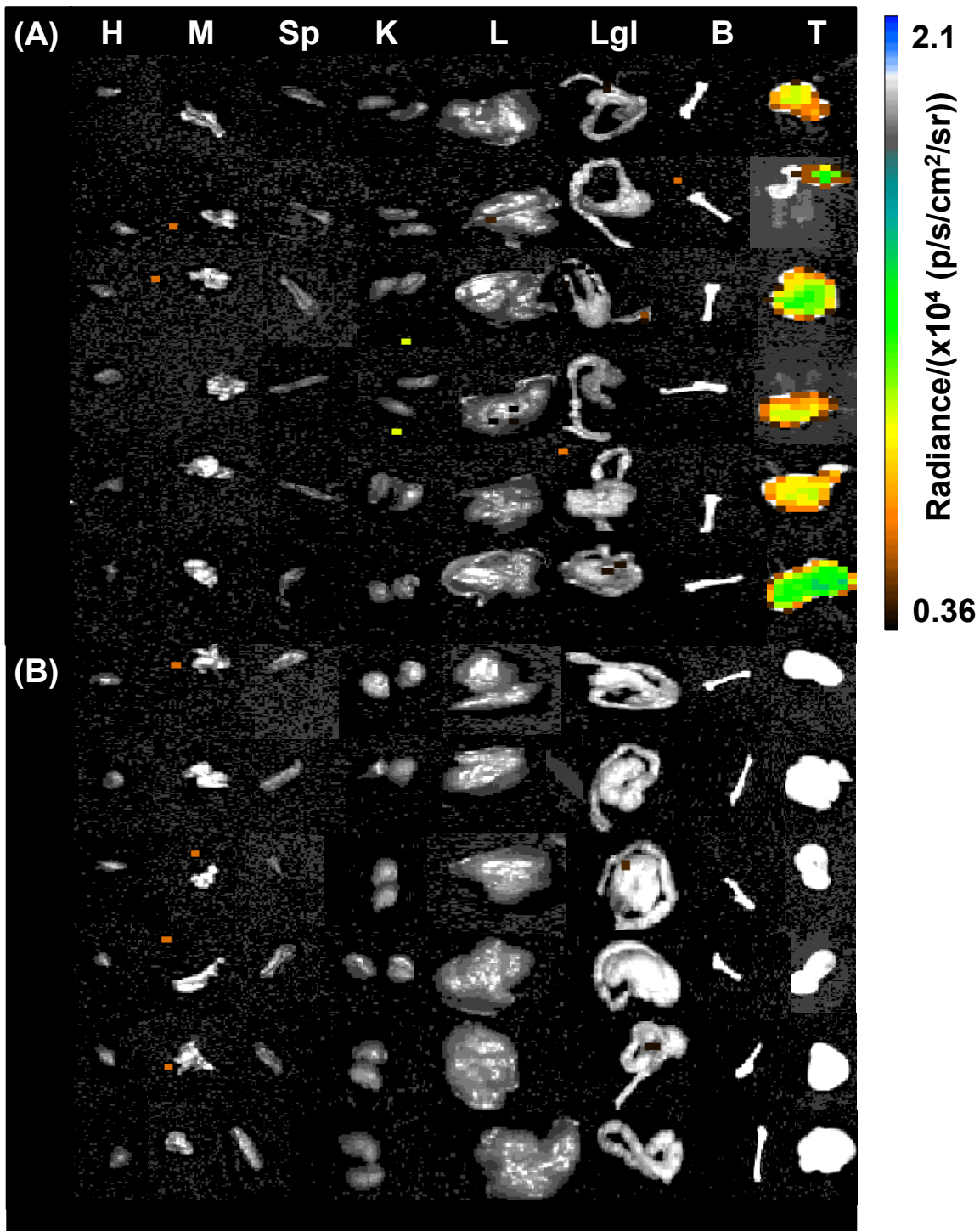


Figure S8. Ex vivo Cerenkov luminescence imaging of selected organs

(A) Ex vivo imaging of the organs detected Cerenkov emissions from the tumors. (B) c(RGDyK) blockade reduces Cerenkov emissions from the tumors and corroborates the *in vivo* results. Organs: Heart (H), Spleen (Sp), Tumor (T), Muscle (M), Kidney (K), Bone (B), Large Intestine (Lgl), Liver (L).

Table S3. Estimated average tumor and kidney dose for animals (n = 6/cohort) receiving ^{225}Ac -DOTA-c(RGDyK)

	Tumor	Kidney
A_0 (μCi)	0.0021	0.0025
λ_e , (h^{-1})	0.01	0.035
T_e (d)	2.89	0.83
Acc ($\mu\text{Ci}\cdot\text{h}$)	0.21	0.071
Dose (rad)	28.78	30.10
Dose equivalent H (Sv)	5.76	6.02

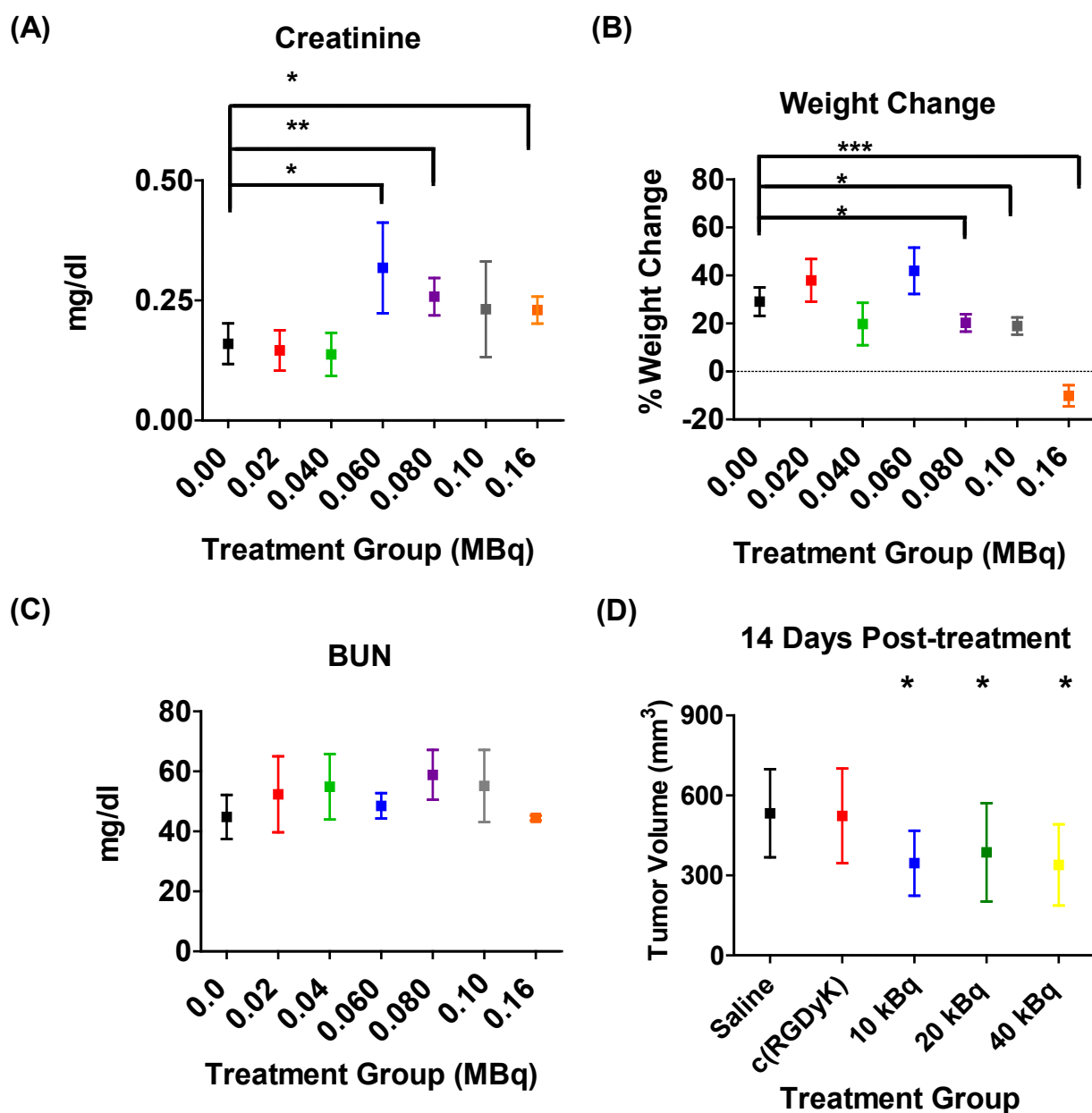


Figure S9. Maximum tolerated dose and preliminary therapy studies of ²²⁵Ac-DOTA-c(RGDyK)

Low doses of ²²⁵Ac-DOTA-c(RGDyK) did not reduce kidney function (**A** and **C**) or cause weight loss (**B**) during the MTD study. (**D**) Animals (n = 10/cohort) treated with ²²⁵Ac-DOTA-c(RGDyK) demonstrated decreased tumor burden compared to control animals (n = 10/cohort). * = p < 0.05, ** = p < 0.01, *** = p < 0.001.

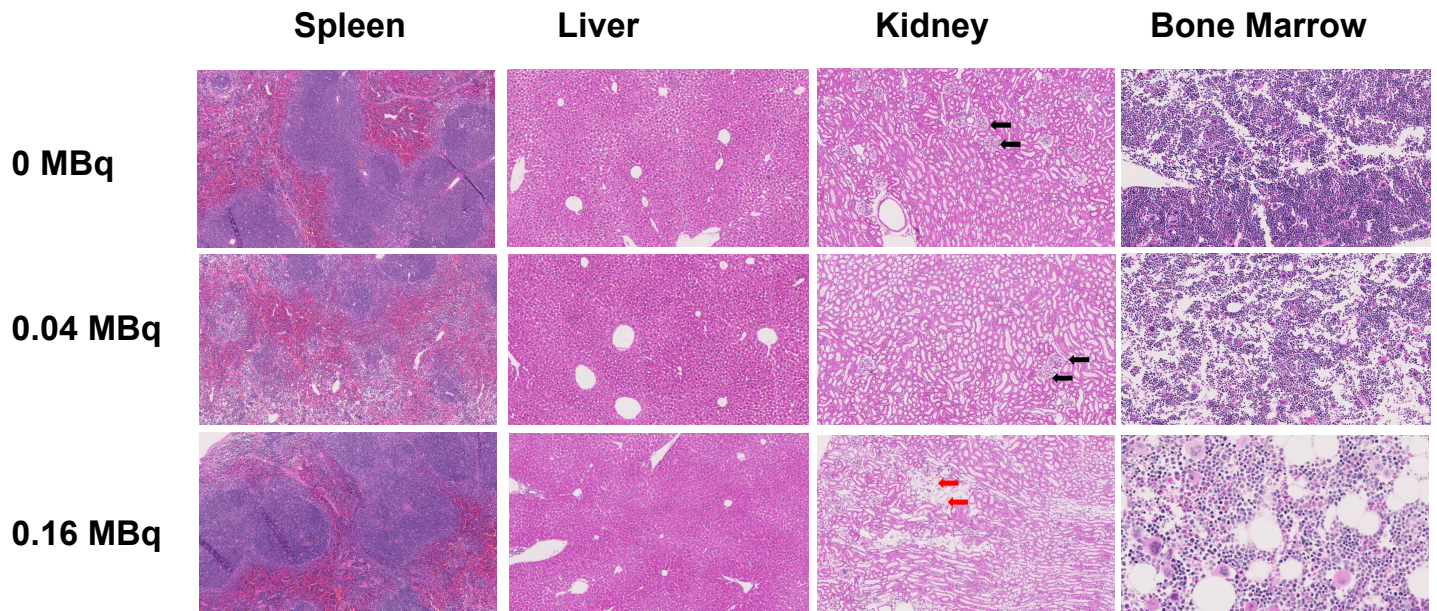


Figure S10. Histology of select tissues from MTD studies

Only animals receiving the largest (0.16 MBq) dose of $^{225}\text{Ac-DOTA-c(RGDyK)}$ demonstrated glomerular loss, which represents irreparable kidney damage (red arrows). Animals receiving the MTD (0.04 MBq) of $^{225}\text{Ac-DOTA-c(RGDyK)}$ did not demonstrate kidney damage. Glomeruli (black arrows) were unremarkable in appearance and resembled the glomeruli (black arrows) of animals receiving saline (0 MBq). All other tissues including spleen, liver and bone marrow were normal. Sections (6 μm) are stained with hematoxylin and eosin. Magnification is 10X for all images except bone marrow (20X).